Steel and Composite Structures, *Vol. 15, No. 3 (2013) 299-322*
DOI: http://dx.doi.org/10.12989/scs.2013.15.3.299

Influence of steel-concrete interaction in dissipative zones of frames: I – Experimental study

Adrian Ciutina [a], Dan Dubina* and Gelu Danku [b]

Department of Steel Structures and Structural Mechanics, Faculty of Civil Engineering – The "Politehnica" University, Str. Ioan Curea No. 1, Timisoara, Romania

(Received October 09, 2012, Revised April 20, 2013, Accepted July 17, 2013)

Abstract. In the case of seismic-resistant composite dual moment resisting and eccentrically braced frames, the current design practice is to avoid the disposition of shear connectors in the expected plastic zones, and consequently to consider a symmetric moment or shear plastic hinges, which occur only in the steel beam or link. Even without connectors, the real behaviour of the hinge may be different from the symmetric assumption, since the reinforced concrete slab is connected to the steel element close to the hinge locations, and also due to contact friction between the concrete slab and the steel element. The paper presents the results and conclusions of experimental tests on composite portal eccentrically braced frames and beam-to-column moment-resisting joints, carried out within the CEMSIG Research Centre of the Politehnica University of Timisoara, in order to check the validity of the assumption stated above. Reference steel and composite specimens with and without connectors in the plastic zones have been tested under monotonic and cyclic seismic type loading.

Keywords: composite beams; plastic hinges; connectors; experimental tests

1. Introduction

In the case of steel structures, the Moment Resisting Frames (MRF) and Eccentrically Braced Frames (EBF) are recognized as efficient systems in dissipating seismic input energy. Both typologies may take advantage of large values of seismic load reduction factors, between 6 and 8. Dual MRF + EBF systems (see Fig. 1) combine the architectural freedom allowed by MRF with the reduction of lateral displacements due to the presence of braces, while keeping their seismic dissipative performance. The use of composite elements such as steel and concrete composite beams or columns may improve structural resistance and rigidity (Elghazouli *et al*. 2008, Simões *et al*. 2001).

Modern seismic norms of composite steel-concrete systems advise to disconnect steel and concrete elements in areas where the plastic hinge is expected to develop, and to consider a symmetric plastic behaviour for the beam, as for the steel section alone. Actually, due to the presence of the reinforced concrete slab (although no connectors are installed) and due to the

*Corresponding author, Professor, E-mail: dan.dubina@ct.upt.ro
[a] Associate Professor, E-mail: adrian.ciutina@ct.upt.ro
[b] Ph.D., E-mail: gelu.danku@ct.upt.ro

http://www.techno-press.org/?journal=scs&subpage=8 ISSN: 1229-9367 (Print), 1598-6233 (Online)

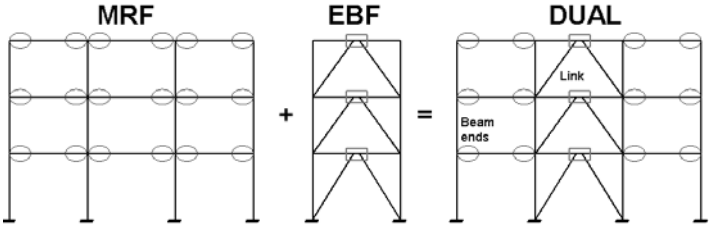

Fig. 1 Plastic zones on MRF, EBF and DUAL MRF + EBF configurations

friction between the steel profile and slab, the plastic hinge on beams will not have a symmetric behaviour under hogging and sagging moments. This could affect the specific seismic design criteria, including the values to be used for the behaviour and overstrength factors.

The composite action of steel beams and concrete slab generally improves the rigidity and resistance of the member, thus calling for careful design and detailing, according to specific sections of EN 1994-1-1 Eurocode 4 (2005) and EN 1998-1 Eurocode 8 (2003). A special attention is to be paid to the detailing of the shear connection between the two materials: steel and concrete (which have a very different elastic and post-elastic behaviour). However, when a composite beams structure is subjected to lateral loads such as earthquakes, the bending moment may suffer sign reversals leading to cracks in the concrete slab, due to tension stresses. Special detailing and requirements are described in the actual seismic design codes for composite beams subjected to seismic loads, such as: (i) special requirements for connecting devices (EN 1998-1 EUROCODE 8 (2003), §7.6.2); (ii) special requirements for the detailing and positioning of the reinforcement of beams adjacent to beam-to-column joints (given in EN 1998-1 EUROCODE 8 (2003), §7.6.2 and Annex C.3.1.2); and (iii) special requirements for design as dissipative or non-dissipative elements.

When using composite beams with Reduced Beam Section (RBS) or composite link elements, the European norms in force are poor in detailing and requirements, practically limiting the composite interaction up to the physical boundaries of the dissipative element according to paragraphs 7.6.2, 7.7.1, 7.7.5 and 7.9.3 of Eurocode 8. Thus, the plasticization is thought of as for a steel element, ignoring the fact that the beam is composite up to the boundaries of the dissipative element. For ordinary design, the influence of the adjacent composite beam on the dissipative capacity of the dissipative element is very difficult to consider.

Generally, the behaviour of composite beams under monotonic loads is very well covered by research worldwide (Johnson and Willmington 1972, Slutter and Driscoll 1963, Oehlers *et al*. 1997). Special detailing has been proposed and implemented in Eurocode 8 for detailing of reinforcement adjacent to beam-to-column joints (Plumier and Doneux 2001a, 2001b, Plumier *et al*. 1998). However, the low-cycle fatigue behaviour of composite beams of EBF and composite beam-to-column joints in MRF subjected to cyclic loads may need special attention in design. As proven by Liang *et al*. (2005) in the case of composite beams, the contribution of the concrete slab in shear is not neglectable and it influences the behaviour of the element. Also, a bad detailing or execution in these cases may lead to modifications of the dissipative element components and consequently to a possible global alteration of the structural seismic capacity (Clifton *et al*. 2011).

The ductile behaviour of steel link elements has been proved by several researchers, by investigating different solutions for best performance. Okazaki *et al*. (2005) have performed a large experimental study, by investigating the disposition and geometrical form of web stiffeners,

and critically analysed the results in regard to AISC provisions. Yurisman *et al*. (2010) showed through experimental and numerical simulations the good capacities of link elements working in shear by using diagonal web stiffeners. Chao *et al*. (2006) investigated the fissure initiation and propagation in stiffened links through experimental and numerical simulations, proposing stiffener configurations that eliminate the presence of welds near *k*-areas. Shayanfar *et al*. (2011) showed the influence of concrete encasement of link web, through experimental investigation.

2. Description of the experimental program

Combining the above-described characteristics of structural systems (MRF and EBF), experimental tests were performed on ductile elements of a dual configuration frame. The experimental investigation was conducted on two ductile sub-structures.

– short links (through one-storey EBFs tests)
– beam-to-column joints of MRF

In both situations, three different beam configurations were considered: (i) the simple steel beam – generically denoted by M; (ii) beam connected with the concrete slab by means of shear connectors (composite cross-section) on the entire span; and (iii) composite beam with connectors suppressed in the potentially plastic region. Another parameter considered was the loading type: monotonic and cyclic respectively.

Experimental specimens were retrieved as subassemblies from a rectangular five-storey reference frame with symmetrical spans on the two directions: two 6 m outer MRF spans and the 4.5 m internal EBF span (see Fig. 2). For the structural analysis, a highly dissipative system was considered, with a seismic load reduction factor $q = 6$. The following features were considered for the equivalent elastic design of elements:

– Location: Bucharest ($a_g = 0.24$ g, $T_C = 1.6$ sec);
– Loads: 4 kN/m^2 permanent load, 3 kN/m^2 live load
– Conditions for steel design and detailing: EN 1993-1-1 and EN 1998-1
– Verification of the collapse mechanism through non-linear push-over analysis

Design requirements led to column elements of HEB 260 (S355 steel) in all locations, while the

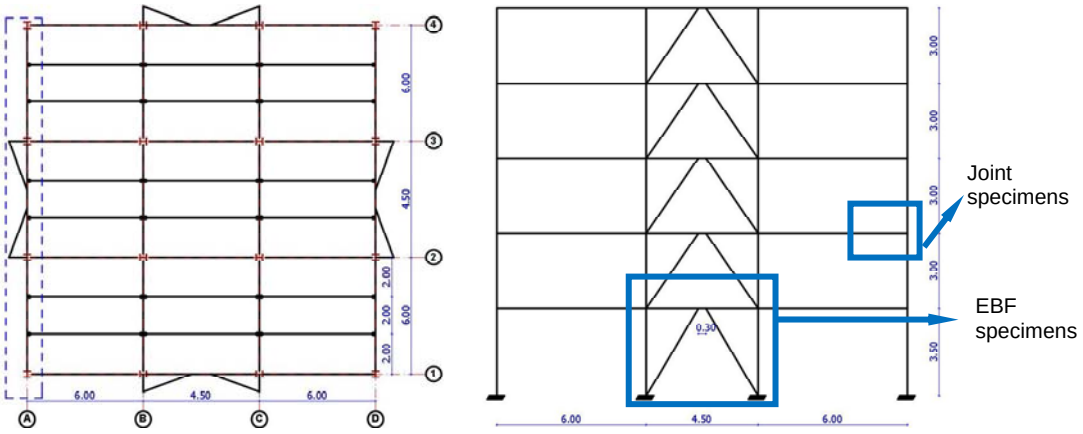

Fig. 2 Reference frame used for production of specimens: plan and front views; retrieved specimens

beam design was different for outer MRF spans (HEA 260 on steel S235) and internal EBF (HEA 200 on S235 steel) respectively. Braces are HEA 180 profiles (steel S355).

3. Experimental Investigation on EBF

3.1 Details of EBF specimens

The EBF set as the base frame for the test series considered the specificity of the CEMSIG laboratory conditions. The figure below shows the main structural dimensions and layout.

Table 1 describes the EBF specimens tested and the configurations thereof, depending on the parameters listed below:

Table 2 shows the mechanical material characteristics of the frame elements:

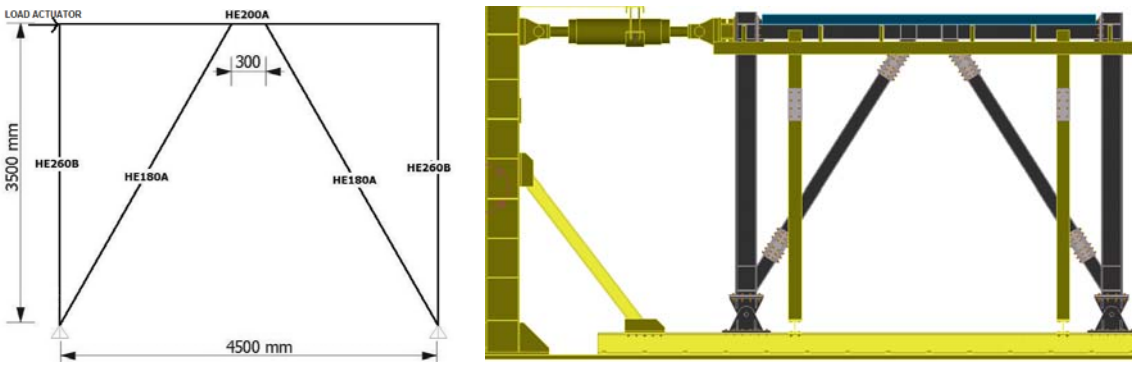

Fig. 3 Dimensions and sections of the base EBF frame (static scheme and testing set-up)

Table 1 Description of the tested EBF specimens

Specimen	Beam type	Type of loading	Connectors on the link	Name of the specimen
1	steel	monotonic	No	EBF_M_LF-M
2	steel	cyclic	No	EBF_M_LF-C
3	composite	cyclic	No	EBF_Comp_LF1
4	composite	cyclic	Yes	EBF_Comp_LF2

Table 2 Nominal values for the tested materials

Element	Profile	Part	Design class	Yield strength [N/mm²]	Ultimate strength [N/mm²]	Elongation at Failure [%]
Beam	HE200A	web	S235	323	475	32.24
		flange		304	434	35.01
Brace	HE180A	web	S355	326	511	29.46
		flange		398	533	36.81
Column	HE260B	flange	S355	283	440	48.06
Concrete Slab	12 cm	-	C20/25	-	23	-

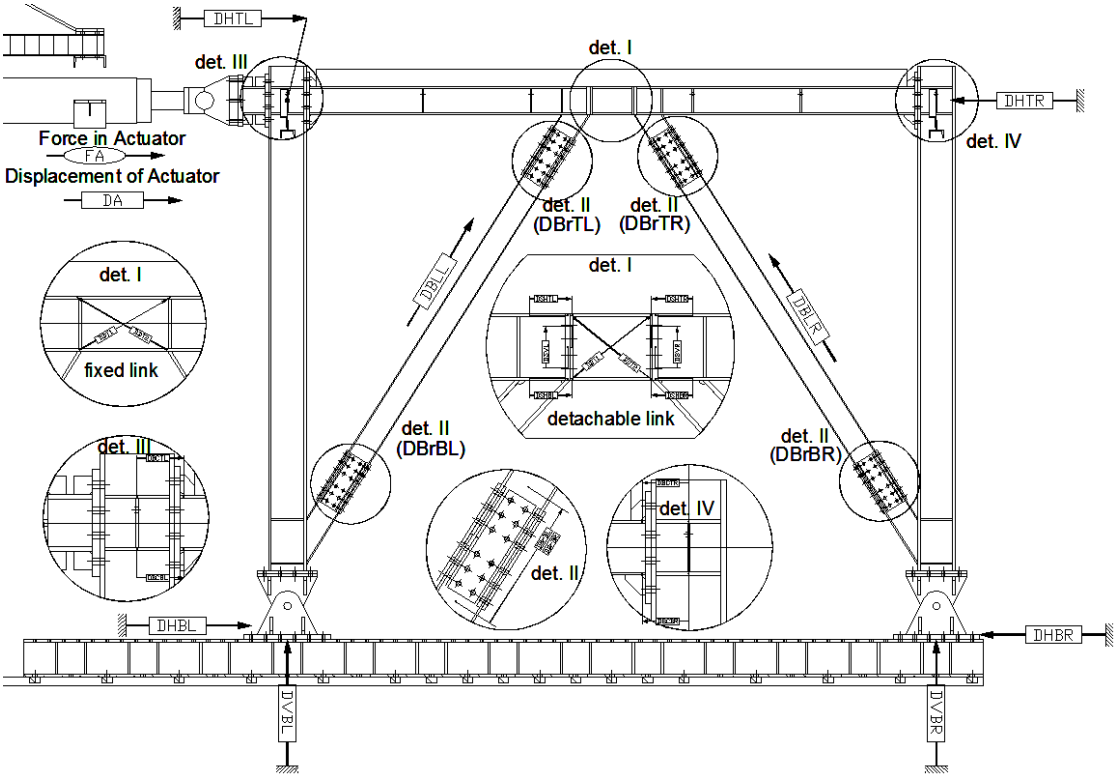

Fig. 4 Global instrumentation of the EBF frame

The lateral load was applied at one end of the top beam through a 100 kN traction/compression actuator. In order to reduce the top force needed for completing the development of the plastic hinge, the tested specimens were pinned at the column base by mechanical hinges. However, as proven by numerical simulations (Goel and Foutch 1984, Ricles and Popov 1987, Stratan and Dubina 2008), the behaviour of the link is not affected by the column-base connection type.

In order to approximate the maximum force needed in the experimental tests, the experimental frame was modelled through a push-over FE analysis (SAP2000), using nominal elastic-plastic characteristics of materials. For this purpose, there was considered the most force-demanding situation, in which the beam was composite over its full length (Danku 2011). In this initial FE model, the composite beam was modelled using the equivalent cross-section characteristics. The resulted maximum load of 780 kN was appropriate for the laboratory facilities.

The load cell integrated in the actuator was used to record the applied force. LVDT displacement transducers were used to monitor different absolute and relative deformations or displacements between different components (see details on Fig. 4). They have been located in key positions according to the type of specimen:

- global displacements of the frame, measured by DHTL, DHTRF, DHTRB transducers, located on top left and right columns;
- web panel distortion of the link: through DDT1 and DDT2 transducers;
- slip and displacements of the non-dissipative elements

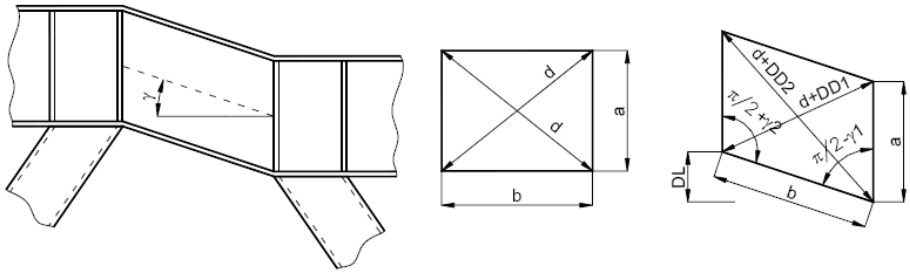

Fig. 5 Deformation of the link element and definition of the distortion angle γ

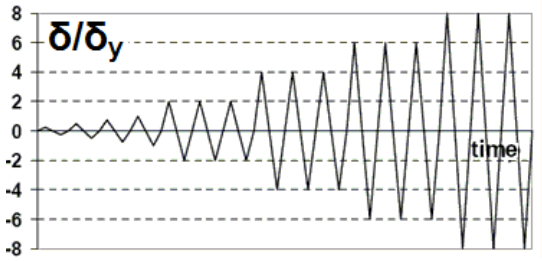

Fig. 6 ECCS cyclic loading procedure

- absolute displacement of pin connections: DHBL, DVBL, DHBR, DVBR;
- slip and elongation of braces and their connections, through DBLL, DBLR, DBrTL, DBrBL, DBrTR, DBrBR transducers

– deformation and rotation of beam-to-column joints: DBCTL, DBCBL, DBCTR, DBCBR transducers.

The total link distortion was accounted for by the angle γ (Stratan and Dubina 2008) as follows (see Fig. 5):

$$\gamma = \frac{\sqrt{a^2 + b^2} \cdot (DD2 - DD1)}{2 \cdot a \cdot b} \tag{1}$$

where $DD1$ and $DD2$ are the recordings given by the two diagonals transducers measuring the link distortion.

The standard ECCS procedure (1986) was applied for loading the monotonic and cyclic tests. From the monotonic base test (EBF_M_LF-M), the yield characteristics (yield displacement δ_y and corresponding force F_y) were computed and used as input data for cyclic tests. The amplitude for the cyclic tests was gradually increased by considering three cycles for each even multiple of δ_y.

3.2 Experimental results

3.2.1 EBF_M_LF-M specimen

As global behaviour, the base steel specimen is characterised as very ductile, the plastic energy dissipating only in the steel link. It was loaded monotonically, up to failure, as shown in Fig. 7. The load increase was limited by the local buckling of the link web panel at about 75 mm, corresponding to a link rotation of about 180 mrad (see Fig. 8). The next chart shows the force –

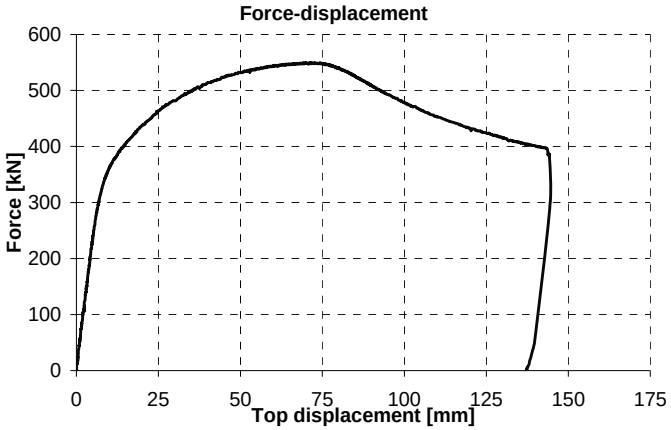

Fig. 7 Load – top displacement curve of the specimen EBF_M_LF-M

top displacement curve of the specimen, where Force represents the load induced by the actuator, while the top displacement is the average displacement given by top transducers, found as

$$D_{tot} = \frac{\left(DHTL + \frac{DHTRF + DHTRB}{2}\right)}{2} - \frac{\left(DHTL + DHBR\right)}{2} \tag{2}$$

The chart in Fig. 8 shows the link distortion – computed according to (1) – versus the shear force of the link. The maximum rotation of almost 280 mrad can be considered as very ductile, this being largely higher than the required values from actual seismic norms, such as P100-1/2006 (2006) and EN 1998-1 (80 mrad) respectively FEMA356 (2000) of 110 mrad corresponding to Collapse Prevention Limit State (CPLS).

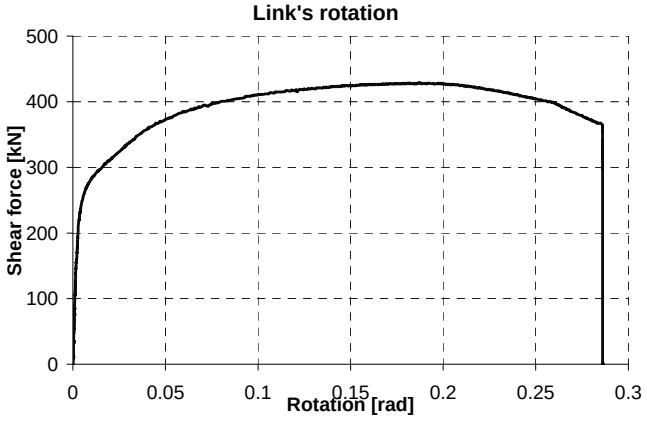

Fig. 8 Shear force-rotation curve of the steel link (specimen EBF_M_LF-M)

The other frame members and components such as beam-to-column connections and braces exhibited only elastic behaviour. Their elastic behaviour was demonstrated by recorded deformations. Among all, the braces proved the largest deformation of 6 mm (see Fig. 9), from which 4 mm was remanent. This fact is explained by the slip in the braces splice-connection clearances (2 mm clearance for each connection).

The loading was stopped at very large inelastic link deformations on the descending branch, at a drop of more than 20% of the maximum load, coincident with stroke limitation of the actuator. Fig. 10 shows (left) the deformed shape of the link at the end of the test and (right) the strain deformation recorded through a 3D surface monitoring system.

3.2.2 EBF_M_LF-C specimen

The response curves obtained in monotonic loading (EBF_M_LF-M specimen) served for the determination of yielding characteristics used in cyclic loading (according to the ECCS procedure). The following values were determined:

– S_{ini} = 48.20117 kN/mm – the initial elastic stiffness of the force-displacement curve;
– F_y = 343 kN – the yielding displacement;
– δ_y = 7.9 mm – the yielding displacement.

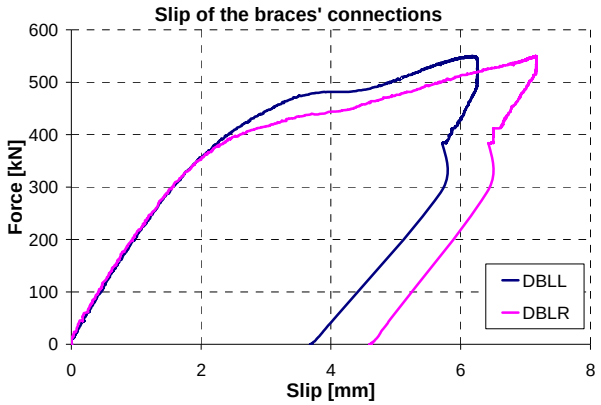

Fig. 9 Total elongation of braces – 4 mm remanent (specimen EBF_M_LF-M)

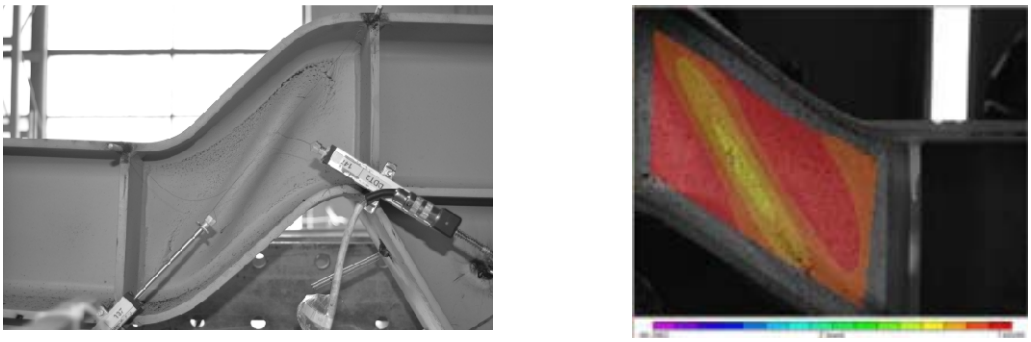

Fig. 10 Dissipative link behaviour in shear for specimen EBF_M_LF-M: pure deformation and strain deformation record for ultimate load

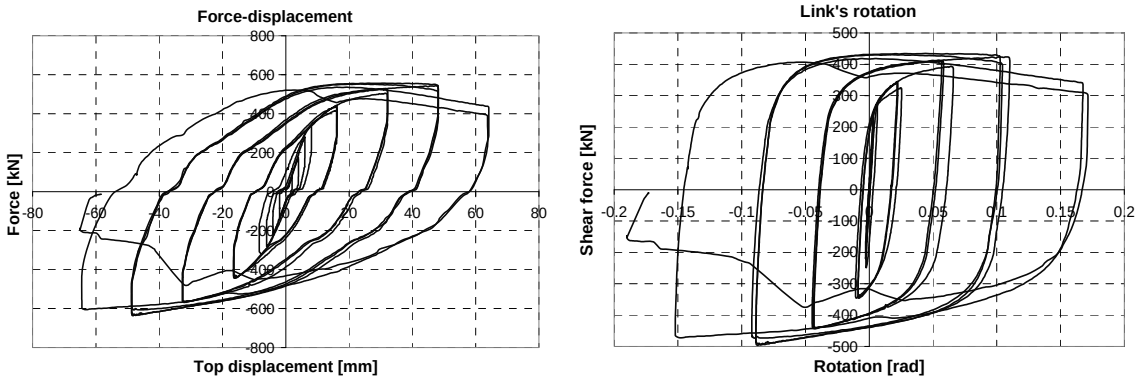

Fig. 11 Global load – top displacement and shear force – link distortion response of EBF_M_LF-C specimen

Fig. 12 Shear failure of EBF_M_LF-C link: pure deformation and strain deformation record for ultimate load

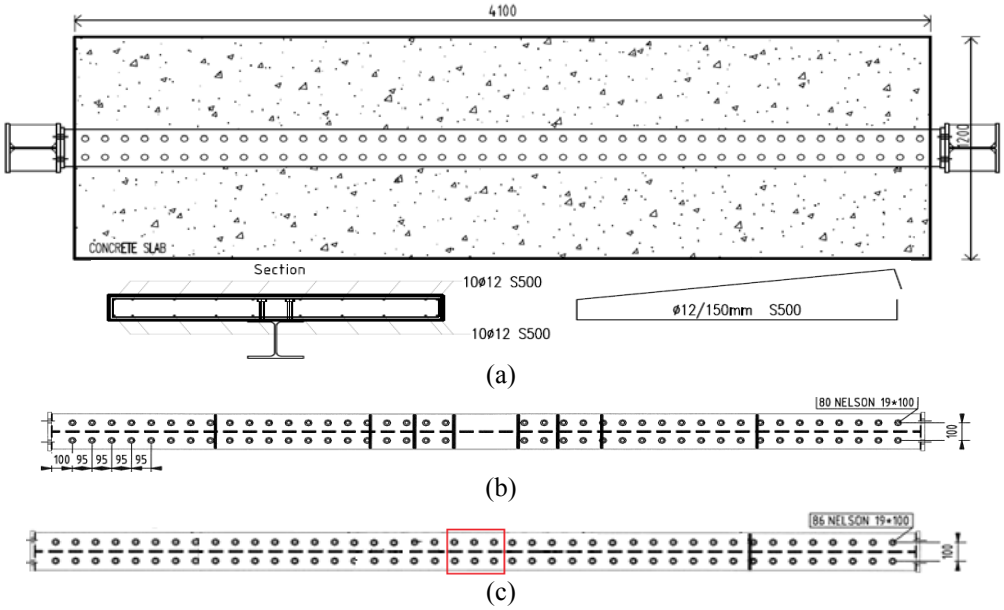

Fig. 13 Details of the reinforcing of the concrete slab and disposition of shear connectors for the composite specimens (top view)

The cyclic loading led to a very small drop in the maximum load (about 20 kN), but also to a great reduction of the distortion capacity (from 280 to 160 mrad). However, the hysteretic curves present stable cycles, as shown in Fig. 11, confirming the recognised good dissipation capacity of EBF link elements.

The failure of the specimen (see Fig. 12) occurred by complete shear of the web panel of the link, which reached 150 mrad for 20% load loss. Diagonal sinusoidal waves formed alternately during the plastic cycles in the web panel.

3.2.3 EBF_Comp_LF1 and EBF_Comp_LF2 specimens

The strength of studs was derived according to the formulae existent in Eurocode 4 for headed stud connectors. Each half of the beam (excluding the link) was considered as a shear span as the moment was constant. The Eurocode 4 requirements to achieve full-interaction of the composite beam lead to the headed stud disposition shown in Fig. 13(b)): 40 pieces of 19 mm in diameter, 100 mm height – placed left and right the link element, disposition which is characteristic to composite beam with non-composite link specimen (EBF_Comp_LF1). In case of composite link specimen (EBF_Comp_LF2), the minimum distance increment of 95 mm characteristic to Φ 19 mm headed studs was kept over the link – see Fig. 13(c)). The reinforcing of the concrete slab (shown in Fig. 14(a)) consisted in longitudinal top and bottom bars Φ 12 mm spaced at 15 cm and tied by transversal stirrups Φ 12 mm spaced at 15 cm.

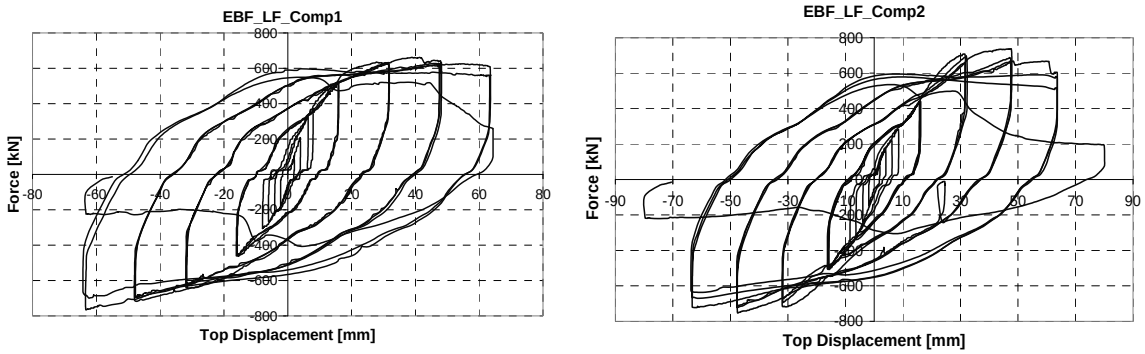

Fig. 14 Top load – lateral displacement response hysteretic curves for specimens LF-Comp 1 and LF-Comp 2

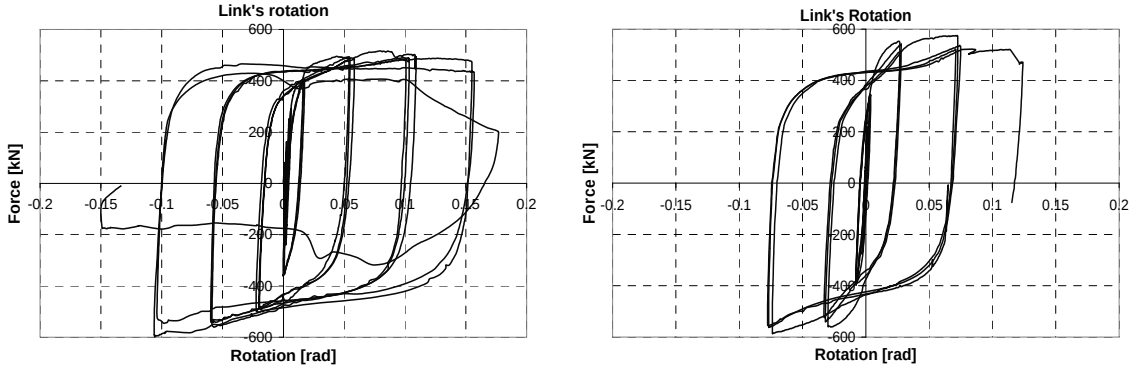

Fig. 15 Shear force – link distortion response hysteretic curves for LF-Comp 1 and LF-Comp 2 specimens

Fig. 16 Damage of the fixed link and concrete slab for EBF_LF_Comp1 (left) and Comp2 (right) specimens

The global behaviour of two specimens is presented in Figs. 14 and 15 through hysteretic response curves (lateral force – top displacement in Fig. 14 and shear force – link distortion in Fig. 15). The shear force – distortion curve presented in Fig. 15 for the LF-Comp 2 specimen is limited to the readings of $6\delta_y$ cycles, due to the alteration of the DDT transducers during the test. However, as general behaviour, both specimens show similar characteristics. Only small differences could be found between the main response parameters: resistance, rigidity and ductility – see Table 3 for numerical values. The values of ultimate link distortions rise to 150 mrad in both situations, which, according to modern seismic norms, is considered sufficient to withstand important values of inter-storey-drift deformations in the case of highly dissipative structures.

Fig. 16 shows the failure conditions for links and the concrete slab. Both specimens experienced high damage in the link panel zone, practically reeling the web plate. Generally, the damage of the slab was concentrated above the link element, developing crack patterns at 45 degrees angles, starting above the link flange corners. No relative deformations (horizontal or vertical) were recorded between the concrete slab and the steel flange. However, the presence of connectors on the link (specimen LF-Comp 2) led to a more important degradation of the concrete slab.

3.3 Appreciation of EBF specimen results

3.3.1 Steel beam, FBP plates and rebars

The synthetic results obtained form the EBF specimens are given in Table 3. The following notations were used:

- $S_{j,link}$ - initial rigidity of the positive branch of the envelope curve;
- V_{max} - maximum shear force during testing;

Table 3 Main synthetic values resulted from EBF experimental tests

Specimen	Initial rigidity $S_{j,link}$ [kN]	Maximum shear resistance V_{max} [kN]	Shear distortion γ at V_{max} [mrad]	Maximum shear distortion γ_{max} [mrad]
EBF_M_LF-M	130460	429	187	286
EBF_M_LF-C	74644	495	87	171
EBF_Comp_LF1	123414	598	105	156
EBF_Comp_LF2	152488	587	74	150*

* *Estimated value*
Note: all values were computed on the maximum envelope curve (cycle 1)

– γ at V_{max} - link rotation corresponding to maximum shear force;
– γ_{max} - maximum link distortion

Figs. 17 and 18 present graphically the main differences between specimen results, in the form of envelope curves: lateral force – top displacement, respectively shear force – panel distortions. The charts follow the stated parameters:

– influence of the composite slab (Fig. 17)
– influence of the loading type (cyclic/monotonic) (Fig. 18)

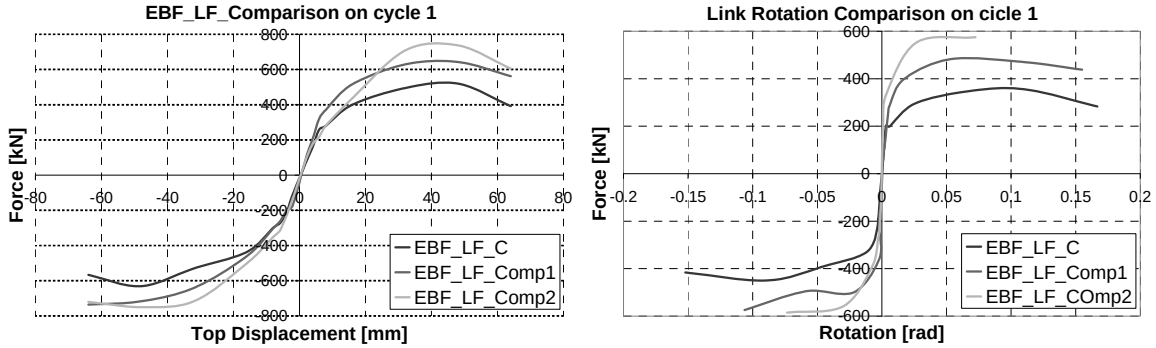

Fig. 17 Influence of the link typology – monotonic curves in cycle 1

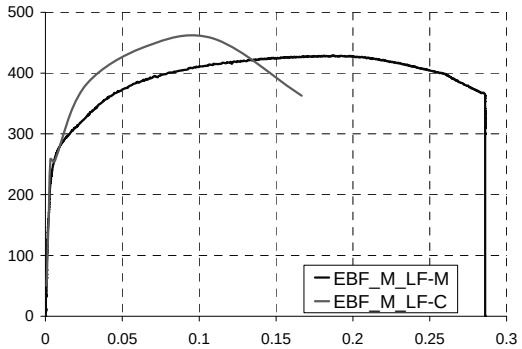

Fig. 18 Influence of cyclic loading – monotonic curves on cycle 1 (steel specimens)

The main difference between results regards the resistance of specimens: both composite tests show higher resistances (up to 20%) as compared to steel specimens. Also, the maximum resistances are similar for full and partial composite specimens (Comp_LF2 and Comp_LF1 respectively), which means that the presence of connectors over the link plays only a secondary role in the global behaviour. This contradicts the normative approach (EN 1998), which suggests that a disconnected dissipative zone leads to a behaviour identical to the one of pure steel.

Another immediate notice is that all specimens exhibited high levels of link distortions, practically meeting the requirements of modern seismic norms (80-140 mrad) for high ductility structures. Concerning the initial stiffness, the computed values show that the rigidity of the cyclic envelope is about 30% higher for composite specimens, compared to the corresponding steel element.

For steel link specimens, the cyclic loading influenced global behaviour, with respect to the following parameters:

- up to 40% decrease in rigidity;
- 15% increase in ultimate resistance;
- the cyclic specimen reached smaller ultimate rotations, up to 171 mrad, compared to 286 mrad recorded in case of monotonic loading

However, the most important conclusion of the link experimental study is that the presence of the slab over the link element will influence noticeably the behaviour of the frame, independently of the link connection with the concrete slab.

4. Experimental investigation on moment-resisting beam-to-column connections

The second source of ductility in the case of dual MRF+EBF structures is located at beam ends of MRF spans, as indicated in Fig. 1. As shown by Chen and Chao (2001), the presence of the concrete slab influences the beam-to-column joint plastic deformation and may lead to premature failure. Ciutina and Dubina (2008) show that the CWP represents a source of high ductility in steel and even composite beam-to-column joints. In the case of end-plate connections, ductility can be achieved by choosing adequate steel grades, end-plate thicknesses and bolts (Girao *et al*. 2004). Other possibilities can be applied in order to enhance the beam-to-column joint ductility, such as the use of RBS (Pachoumis *et al*. 2010) or the use of dissipative devices such as fuses (Castiglioni *et al*. 2012). The experimental study presented herein is focused on the use of RBS for concentrated plasticity and different interactions with the concrete slab.

4.1 Specimen description and testing set-up

Fig. 19 shows the testing set-up: the column, here disposed horizontally, was pinned at both ends (at half-story distances) while the beam was vertical and loaded in bending by the actuator, at the beam top. A lateral-restraining frame was considered, for keeping the in-plane post-elastic behaviour of the beam.

The following cross-section and material characteristics were considered for beam-to-column specimens:

- column: HEB260 (S355) and HEB300 (S460);
- beam: HEA260 (S235);
- typology of the connection: direct welding of the beam on the column flange through full penetration weld (see Fig. 20(a) for welding detail), with reduced beam section (RBS) near

the connection. The design of the RBS was performed according to EN1998-3:2005, Annex B, section 5.3.4, and the resulting geometric properties were detailed in Fig. 20(b).

The connection was loaded in bending through the actuator located at the top of the beam. The load cell attached to the actuator measured the force during the test. The general instrumentation of the joint specimens is shown in Fig. 21. Additionally, displacement transducers were placed for measuring the following data:

- beam top displacement - by means of DTF and DTB transducers;
- local rotations, deformations and distortions in the dissipative elements: RBS, web panel of the column, welds (through DBLL, DBLR, DDT1, DDT2, DWL, DWR transducers);
- local slip in pins through DHBL, DVBL, DHBR, DVBR transducers

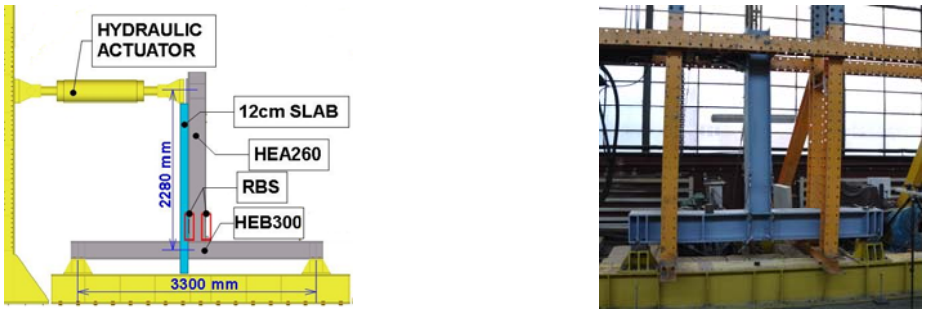

Fig. 19 Joint location and testing set-up

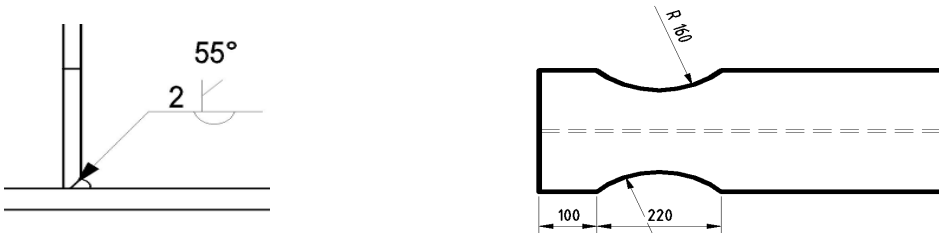

(a) (b)

Fig. 20 Detail of the beam-to-column weld and geometry of the reduced beam section

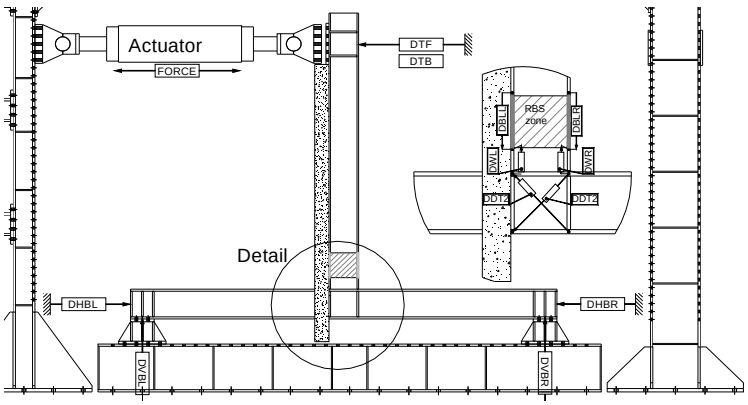

Fig. 21 RBS specimen instrumentation

The following formulae were used for computing different rotations (the measurement of a certain transducer is indicated by its name):

– RBS distortion (h_b and t_{fb} are the height and the flange thickness respectively):

$$\gamma_{RBS} = \frac{(DBLL - DBLR)}{h_b - t_{fb}} \tag{3}$$

– Welded connection:

$$\gamma_{RBS} = \frac{(DWL - DWR)}{h_b - t_{fb}} \tag{4}$$

– Column web panel distortion in shear (h_c is the column height):

$$\gamma_{col.web} = \frac{\sqrt{a^2 + b^2} \cdot (DDT2 - DDT1)}{2ab} \tag{5}$$

where

$$a = h_c$$

$$b = h_b - t_{fb}$$

Table 4 shows the name and characteristics of RBS joint specimens. The main parameters focus on the influence of the concrete slab and the type of loading (monotonic or cyclic).

Before testing the specimens, material samples were tested in order to check the steel quality for steel elements (tensile tests) and concrete elements (in compression). Table 5 shows the design and actual main mechanical characteristics of materials (confirming the minimum resistance requirements).

Table 4 Description of RBS specimens

Specimen	Beam type	RBS	Loading type	Connectors over RBS zone	specimen name
1	steel	Yes	monotonic	No	DB-M
2	steel	Yes	cyclic	No	DB-C
3	composite	Yes	cyclic	No	DB-Comp1
4	composite	Yes	cyclic	Yes	DB-Comp2
5	steel	Yes	cyclic	No	DB-C RLD
6	composite	Yes	cyclic	Yes	DB-Comp RLD

Table 5 Description of RBS specimens

Element	Design characteristics	Actual characteristics		
		f_y / f_c [N/mm^2]	f_u [N/mm^2]	Elongation [%]
Beam	S235	263	396	43.82
Column (Spec.1-4)	S355	283	440	48.06
Column (Spec.5-6)	S460	440	632	32.21
Concrete	C20/25	23	N/A	N/A

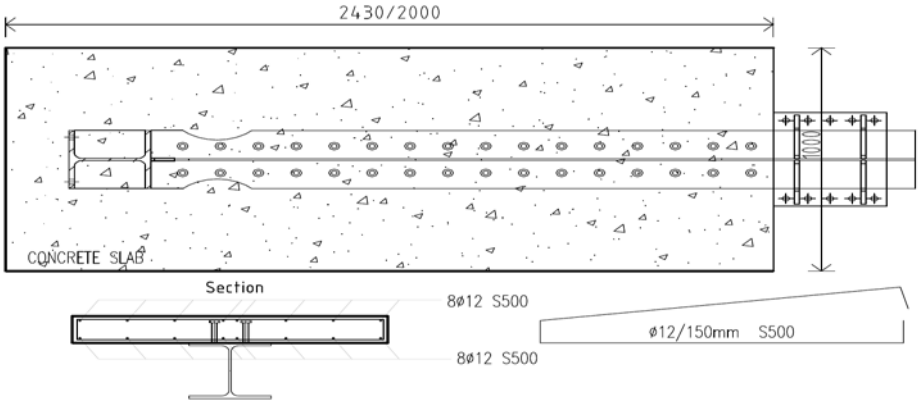

Fig. 22 Detailing of reinforcing of concrete slab over beam-to-column joint

The concrete slab for composite specimens was designed in the same manner as in case of EBF specimens (see paragraph 3.2 - 12 cm thickness) and respects the same disposition of longitudinal and transversal rebars (see Fig. 22), but adapted for a concrete width of 1m. The reinforcing of the beam-to-column composite joint was verified to EN1998-1: Annex C prescriptions.

4.2 Experimental results

4.2.1 DB-M specimen

The test was carried out until important plastic deformations were recorded. The termination of the test was practically due to the reaching of the actuator displacement limit. Based on the force-top displacement curve, the yield displacement d_y, yield force F_y and the initial rigidity were determined and used for piloting the cyclic specimens. The yield point was determined at the intersection of the initial elastic rigidity with a tangent to the graph, with a rigidity equal to 10% of the elastic one.

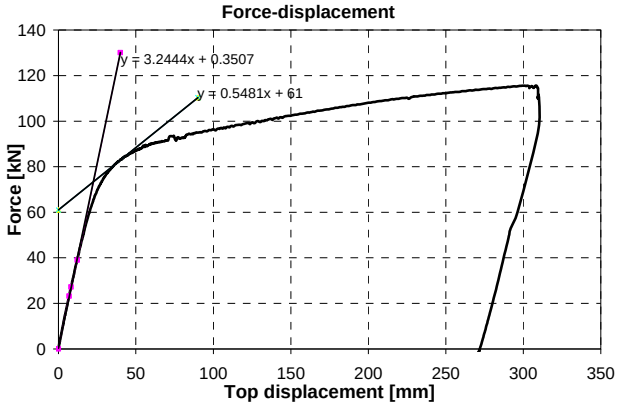

$S_{j,ini}$ = 3.24 kN/mm
δ_y = 22.2 mm
F_y = 72 kN

Fig. 23 Load-displacement curve of DB-M specimen

Although in this case the beam is the dissipative element, due to a smaller resistance of the steel material in the column, the joint plasticization was shared between two ductile components: the RBS zone through flexure, and Column Web Panel (CWP) in shear. First, the plasticization was recorded in the CWP, beginning at relatively small deformations – 25 mm in the top loading actuator. Once the CWP resistance increased through strain-hardening, the RBS plasticised, beginning at values of the top displacement of about 35 mm.

Fig. 24 shows a graphical comparison between the total joint rotation (recorded through DTF, DTB transducers) and the local RBS rotation. It results very clearly that a large amount of final rotation is assigned to components other than the RBS, maily to the CWP in shear. However, the total RBS rotation could be judged as high, exceeding 80 mrad for RBS solely.

For Fig. 24, a representation of force was chosen instead of moment (usually used), for a unitary representation: the level arms which multiply the force are significantly different in the RBS centre (1.96 m) and the CWP centre (2.28 m) respectively.

Fig. 25 shows the behaviour of the plasticized zones in the specimen during the test and the failure pattern, by local buckling of the beam's flange in the RBS.

A very important notice should be added in the conclusion, for the first specimen of RBS joints: due to the fact that the steel quality of the column was lower than the one ordered (S275 –

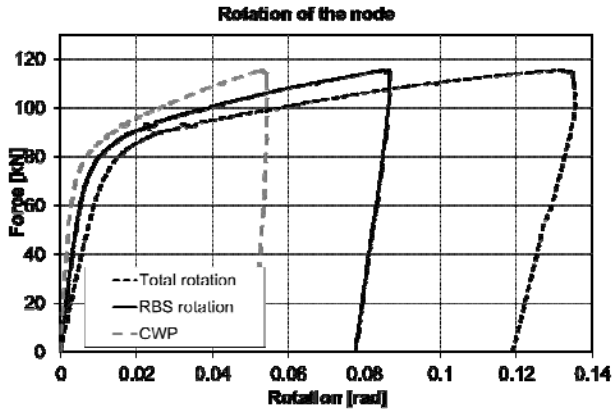

Fig. 24 Force-rotation curve of the steel joint with reduced beam section

Fig. 25 Failure of the DB-M specimen

supplied instead of S355 – ordered, according to Table 5), the column web panel became the component with the lowest resistance. Consequently, it highly influenced the distribution of plastic deformations within the joint between RBS and CWP.

4.2.2 DB-C specimen

The DB-C steel specimen was cyclically loaded, with an identical configuration with the base DB-M specimen. The cyclic loading pattern, according to the ECCS protocol, was set after determining the yield displacement. A value of 20 mm was considered for d_y, as determined from DB-M specimen test results and their interpretation.

The global joint rotation shown in Fig. 26 could be considered as satisfactory, reaching 80 mrad, with the major observation that this is due primarily to CWP plastification, as in case of DB-M specimen. The specimen failure mode was by fracture of the beam-to-column flange welds (recorded at an increment of $8 \times dy$ - third cycle), practically coincident with the maximum actuator stroke limit.

4.2.3 DB-Comp1 and DB-Comp2 specimens

The composite specimens use the same joint typology as the steel (DB-M and DB-C) ones. However, for the composite specimens, the steel beam is connected to a 12 cm slab, detailed in

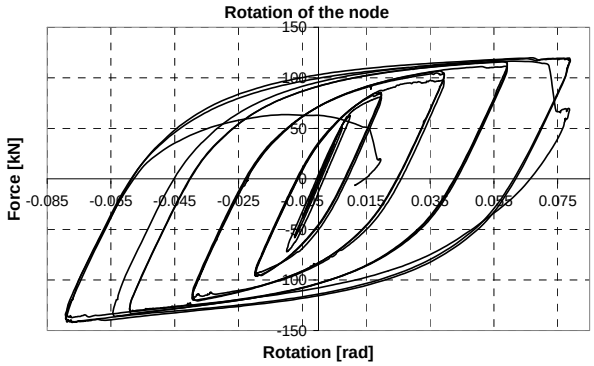

Fig. 26 Force – total rotation curve of the DB-C specimen

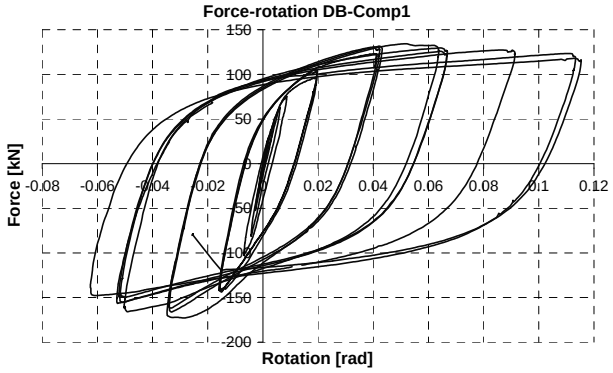

Fig. 27 Total force-rotation curve for the DB-Comp1 specimen

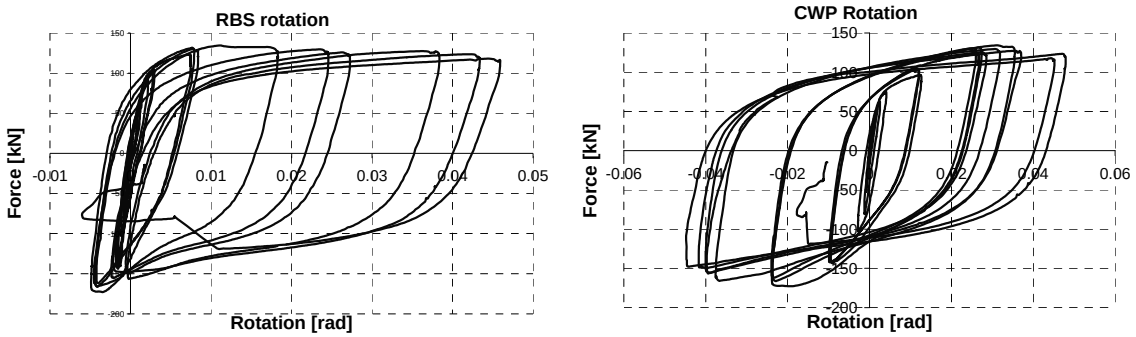

(a) (b)

Fig. 28 Deduction of RBS and CWP rotations for DB-Comp1

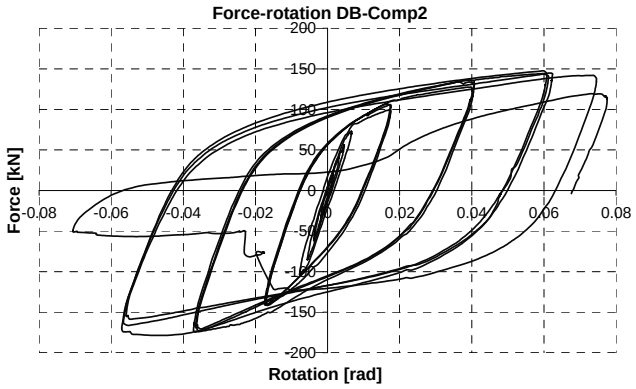

Fig. 29 Force-rotation curves for the DB-Comp2 specimen

paragraph 4.1. The main difference between the DB-Comp 1 and DB-Comp 2 specimens is represented by the steel-concrete interaction above the RBS zone. In the case of the DB-Comp1 specimen, no connectors are disposed over the RBS zone, while, for the DB-Comp2 specimen, the shear connection is continuous over the top flange of the beam.

The loading of the specimens was satisfactory up to the third cycle for an increment of $8 \times dy$ (see Fig. 27), when, like in the case of the cyclic steel specimen, the welds between the flange of the beam and the flange of the column cracked. The force-rotation hysteretic curves for the two composite joints are shown in Figs. 27 and 28:

The total rotation of the joint (Fig. 27) is actually the sum of CWP and RBS zones rotations. The asymmetry of the global curve is due to the RBS zone (Fig. 28(a)) which developed plastic rotation only for hogging (concrete in tension), while the plasticization in sagging was prevented by the higher resistance of the composite section. On the contrary, the CWP rotation is symmetrical (Fig. 28(b)), without any influence from the concrete slab. The total plastic hogging rotation was practically equally shared between the two components (40 mrad).

The DB-Comp2 specimen behaved similarly and confirmed the above remarks. However, this time the cycles were more stable although the failure was recorded at the same displacement amplitude and by similar weld failure (see Fig. 29). In both cases, the concrete slab was crushed at

the interface with the column flange in compression, while, in tension, fissures formed starting from column flange corners (see Fig. 30). However, the concrete slab was much more affected in the case of the DB-Comp1 specimen, as shown in Fig. 30(a), which demonstrates that the steel-to-concrete connection remains effective although shear connectors are not provided near the column.

Fig. 31 presents in comparison the moment-rotation envelopes for DB cyclic loaded specimens. It becomes obvious that, as in the case of EBF tests the global behaviour of composite specimens is very similar, regardless of the presence of connectors over the dissipative zone (RBS).

In comparison with the steel specimen, the composite ones show higher stiffness, especially with regard to the hogging behaviour (42.95 kNm/mrad for DB-Comp1 and 36.72 kNm/mrad for DB-Comp2 in regard to 25.38 kNm/mrad for DB-M). The maximum resistance is also significantly higher for composite specimens:

– 321.98 kNm for composite and 268.69 kNm for steel specimens in hogging bending;
– 392.90 kNm for composite and 321.67 kNm for steel specimens in sagging bending.

For all specimens, the ductility was limited by the premature failure of welds.

4.2.4 Cyclic testing of the beam-to-column joints with RBS- DB-C_RLD & DB-Comp_RLD

Because the purpose of the initial RBS specimens was not fully achieved (dissipation only in the RBS zone), the joint test series was completed by two new specimens, namely DB-C_RLD

(a) (b)

Fig. 30 (a) Failure of specimens DB-Comp1; and (b) DB-Comp 2

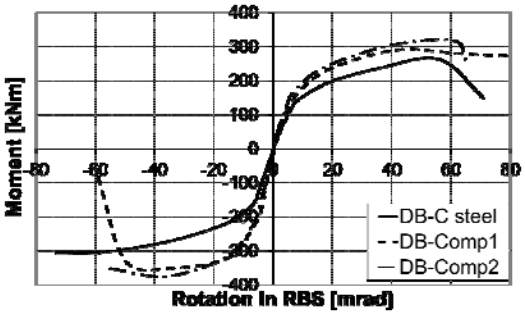

Fig. 31 Comparison of the moment-rotation envelope curves for the tested nodes

(steel specimen) and DB-Comp_RLD (composite specimen), both tested cyclically. In this configuration, the beam section was kept (HEA260), while the column was replaced by a HE300B profile in S460 steel grade.

Consequently, for this new series of tests, the expected failure type was reached in both cases, through ductile plastification of the RBS and gradual reduction of the joint resistance. No important plastification of the CWP in shear was recorded. In the case of the composite specimen, the buckling of the upper flange was avoided, due to the presence of the concrete slab. However,

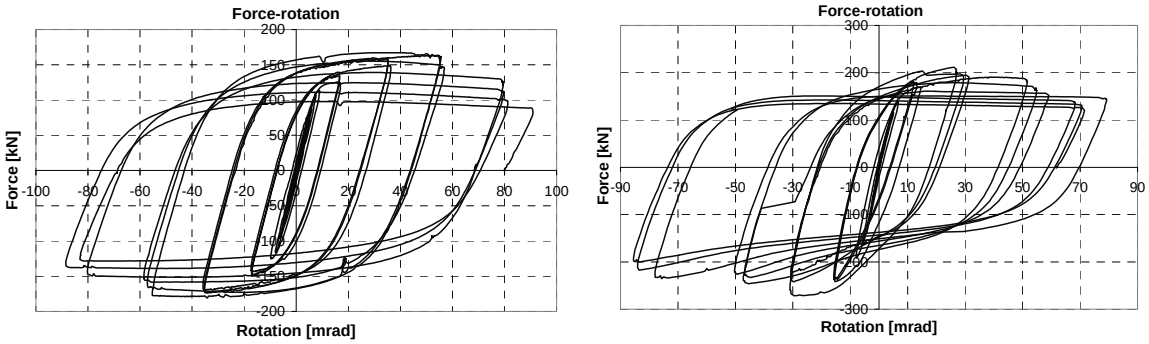

(a) (b)

Fig. 32 (a) Force-rotation curve of the steel specimen DB-C_RLD; and (b) respectively composite DB-Comp_RLD; specimens, under cyclic loading

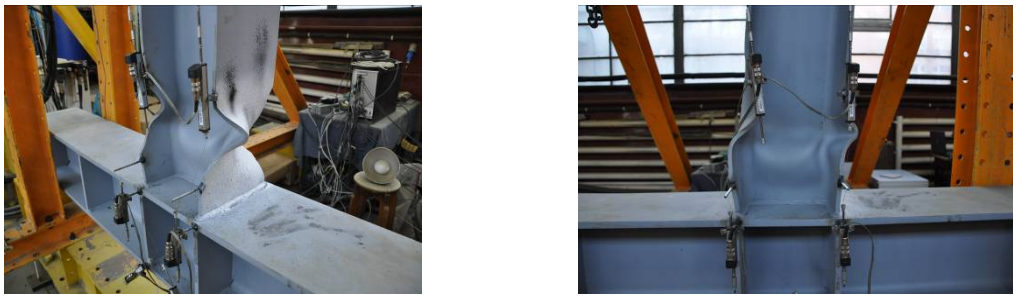

Fig. 33 Failure of the DB-C RLD specimen through plastic hinges in RBS

Fig. 34 Crushing of concrete and buckling of the compressed flange, and for the DB-Comp_RLD specimen

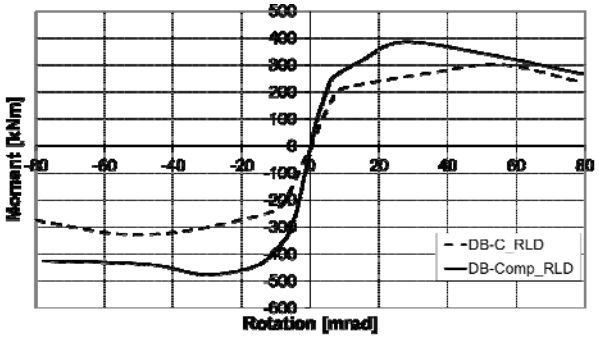

Fig. 35 Comparison of the force-displacement envelope curves for DB-C_RLD and DB-Comp_RLD specimens

its resistance gradually degraded during the plastic cycles, by concrete degradation due to fissures recorded parallel to the column flange, when the slab was in tension, and, respectively, by crushing along the fissures already formed in tension, when the slab was in compression.

The charts plotted in Fig. 32 show the hysteretic curves in terms of applied force and total joint rotation. The total rotation – higher than 70 mrad in both cases – is due almost exclusively to the RBS plasticization. However, high degradation was recorded in the concrete slab around the column zone, in which the concrete was crushed in reversal cycles and massively fell off.

The results of the new series of DB specimens confirmed the conclusions of the first test series. Comparing the envelope force-rotation curves (see Fig. 35) similar rotation capacities were noticed (up to 70 mrad), and higher resistances and rigidities for the composite specimen, especially in negative bending (slab under compression), as compared to steel bare connection.

5. Conclusions

The main objective of the experimental analysis regarded the influence of the steel-to-concrete interaction on the cyclic response of dissipative zones formed in moment resisting and eccentrically braced frames. The concerned zones are the beam ends, in the case of MRF's, and the links, in the case of EBF's. The following main conclusions could be drawn from the study:

- The simple disconnection of the steel beam from the concrete slab over the dissipative zone is not sufficient to ensure a pure steel-like behaviour of the element. The resulted behaviour is practically very close to that of a full-composite specimen;
- In both situations the composite aspect improves the global resistance and stiffness characteristics of the dissipative zones, while maintaining the ductile nature of the solution. However, the composite behaviour should be considered in the design of elements without connectors over the dissipative zone;
- A very careful detailing and execution should be applied to beam-to-column joints and links in order to reach the desired levels of ductility and resistance. On the contrary, the steel grade mismatch could change the plasticization order, while the defective execution of welds may lead to the brittle failure of the element;
- The reduced beam section solution remains effective in the composite configuration, but the presence of the concrete slab changes the failure mode: the top flange is restrained in

buckling, while the concrete slab is degraded by cyclic tension-compression alternating forces.

Acknowledgements

The research programme was financed by the Romanian Ministry for Education and Research through the research grant PNCDI II "Partnerships", contract no. 31.042/2007 Structural systems and innovative technological solutions for the protection of buildings subjected to extreme actions in the context of sustainable development PROACTEX.

References

Castiglioni, C., Kanyilmaz, A. and Calado, L. (2012), "Experimental analysis of seismic resistant composite steel frames with dissipative devices", *J. Construct. Steel Res.*, 1-12.

Chao, S-H., Khandelwal, K. and El-Tawil, S. (2006), "Ductile web fracture initiation in steel shear links", *J. Struct. Eng. – ASCE*, **132**(8), 1192-1200.

Chen, S-J. and Chao, Y.C. (2001), "Effect of composite action on seismic performance of steel moment connections with reduced beam sections", *J. Construct. Steel Res.*, **57**(4), 417-434.

Ciutina, A.L. and Dubina, D. (2008), "Column web stiffening of steel beam-to-column joints subjected to seismic actions", *ASCE, J. Struct. Eng.*, **134**(3), 505-511.

Clifton, C., Bruneau, M., MacRae, G., Leon, R. and Fussell A. (2011), "Steel structures damage from the Christchurch Earthquake of February 22, 2011, NZST", *Bulletin of the New Zealand Soc. Earthq. Eng.*, **44**(4), 297-318.

Danku, G. (2011), "Study of the development of plastic hinges in composite steel-concrete structural members subjected to shear and/or bending", Ph.D. Thesis, Politehnica University of Timisoara.

Elghazouli, A.Y., Castro, J.M. and Izzuddin, B.A. (2008), "Seismic performance of composite moment-resisting frames", *Eng. Struct.*, **30**(7), 1802-1819.

EN 1994-1-1 EUROCODE 4 (2005), Design of composite steel and concrete structures, Part 1.1. General rules and rules for buildings, Brussels, CEN, European Committee for Standardisation.

EN 1998-1 EUROCODE 8 (2003), Design of structures for earthquake resistance, Part 1. General rules, seismic actions and rules for buildings, Brussels, CEN, European Committee for Standardisation.

European Convention for Constructional Steelwork (1986), Technical Committee 1, TWG 1.3 – Seismic Design, No. 45, Recommended Testing Procedures for Assessing the Behaviour of Structural Elements under Cyclic Loads.

FEMA 356 (2000), Prestandard and Commentary for the Seismic Rehabilitation of Buildings, Federal Emergency Management Agency, Washington, D.C., November.

Girao, A-M., Bijlaard, F.S. and da Silva, L.S. (2004), "Experimental assessment of the ductility of extendedend plate connections", *Eng. Struct.*, **26**(9) 1185-1206.

Goel, S.C. and Foutch, D.A. (1984), "Preliminary studies and test results of eccentrically braced full-size steel structure", *US-Japan Cooperative Earthquake Research Program Utilizing Large Scale Test Facilities, Proceedings of the 16th Joint Meeting on Wind and Seismic Effects*, UJNR, Maryland, May.

Johnson, R.P. and Willmington, R.T. (1972), "Vertical shear in continuous composite beams", *Proceedings of the Institution of Civil Engineers*, **53**(2), 189-205, September.

Liang, Q., Uy, B., Bradford, M. and Ronagh, H. (2005), "Strength analysis of steel-concrete composite beams in combined bending and shear", *J. Struct. Eng. – ASCE*, **131**(10), 1593-1600.

Oehlers, D.J., Nguyen, N.T., Ahmed, M. and Bradford, M. (1997), "Partial interaction in composite steel and concrete beams with full shear connection", *J. Construct. Steel Res.*, **41**(2-3), 235-248.

Okazaki, T., Arce, G., Ryu, H.-C. and Engelhardt, M.D. (2005), "Experimental study of local buckling, overstrength, and fracture of links in eccentrically braced frames", *J. Struct. Eng. – ASCE*, **131**(10), 1526-1535.

P100-1-2006 (2006), P100-1 Cod de proiectare seismic – Partea I – Prevederi de proiectare pentru cladiri, indicativ P 100-1/2006, Romanian Institute of Standardization.

Pachoumis, D.T., Galoussis, E.G., Kalfas, C.N. and Efthimiou, I.Z. (2010), "Cyclic performance of steel moment-resisting connections with reduced beam sections - experimental analysis and finite element model simulation", *Eng. Struct.*, **32**(9), 2683-2692.

Plumier, A. and Doneux, C. (2001a), "Seismic behaviour and design of composite steel concrete structures", European Comission – Training and Mobility of Researchers – Programme Innovative Concepts in Seismic Design "ICONS" Project, May.

Plumier, A. and Doneux, C. (2001b), "European developments of seismic design guidelines for composite steel concrete structures", *Proceedings of International Conference of Steel and Composite Structures ICSCS'01*, Pusan, June.

Plumier, A., Doneux, C. and Bouwkamp, J.G. (1998), "Slab design in connection zone of composite frames", *Proceedings of the 1998 Annual Technical Session & Meeting of the Structural Stability Research Council*, 21-23, Atlanta, September.

Ricles, J.M. and Popov, E.P. (1987), *Experiments on Eccentrically Braced Frames with Composite Floors*, Earthquake Engineering Research Centre, University of California, Berkeley, CA.

Shayanfar, M.A., Barkhordari, M.A. and Rezaeian, A.R. (2011), "Experimental study of cyclic behavior of composite vertical shear link in eccentrically braced frames", *Steel Compos. Struct., Int. J.*, 12(1), 13-29.

Simões, R., da Silva, L.S. and Cruz, P. (2001), "Cyclic behaviour of end-plate beam-to-column composite joints", *Steel Compos. Struct., Int. J.*, **1**(3), 355-376.

Slutter, R.G. and Driscoll, G.C. Jr. (1963), "Flexural strength of steel and concrete composite beams", *Fritz Laboratory Reports*, Paper 1806.

Stratan, A. and Dubina, D. (2008), "Removable bolted links for eccentrically braced frames", *Proceedings of the International Symposium "Urban Habitat Constructions under Catastrophic Events"*, Malta, October, COST Action C26, Editors: Mazzolani, Mistakidis, Borg, Byfield, De Matteis, Dubina, Indirli, Mandara, Muzeau, Wald, Wang, 181-186, ISBN 978-99909-44-42-6.

Yurisman, Budiono, B., Moestopo, M. and Suarjana, M. (2010), "Behavior of shear link of WF section with diagonal web stiffener of Eccentrically Braced Frame (EBF) of steel structure", *ITB J. Eng. Sci.*, **42**(2), 103-128.

BU